To appear in:

Iranian Journal of Catalysis (IJC)

Online ISSN: 2345-4865 Print ISSN: 2252-0236

Received: 13 January 2026

Revised: 02 April 2026

Accepted: 16 April 2026

Published Online: 28 July 2026

DOI: 10.57647/ijc.2026.1603.23

RESEARCH PAPER

A Novel Solid Acid Catalyst for the Esterification Reaction of n-butanol and Acetic Acid: Sulfated Ceria and Amorphous Silica

Kum-Hyok Song, Myong Yun, Un-Ha Kim*, Se-Ok Pak

Faculty of Chemistry, Kim Il Sung University, Pyongyang, Democratic People's Republic of Korea

* E-mail: uh.kim0102@ryongnamsan.edu.kp (U. H. Kim)

(https://orcid.org/0009-0004-6774-188X)

Abstract

A novel solid acid catalyst based on ceria and amorphous silica was successfully prepared by coprecipitation-impregnation method with ceric sulfate and sodium metasilicate. This research aimed to examine the availability of sulfated ceria and amorphous silica catalyst for the synthesis of n-butyl acetate. The catalyst was characterized by means of XRD, N_2 sorption, SEM, Hammett Indicator titration, FT-IR, TG-DTA. The experimental results show that this catalyst has the high catalytic activity and reusability because of the strong acidity and good thermal stability of sulfated ceria. With the catalyst, the maximum conversion of acetic acid was obtained as 97.3% under the optimum conditions (molar ratio of n-butanol to acetic acid 1.6, catalyst amount 2.3 wt%, reaction temperature 120 °C, reaction time 120 min). Moreover, even at temperatures higher than 120 °C, any by-products were not formed and the conversion of acetic acid was up to 90% for five cycles.

We confirmed that sulfated ceria and amorphous silica-based solid acid catalyst could be used effectively for the esterification reaction.

Keywords: Ceria, Silica, Solid acid, Esterification

1. Introduction

In the esterification reactions, conventional homogeneous acid catalysts, such as sulfuric acid and hydrochloric acid, have inevitable drawbacks because of their severe corrosion and environmental problems [1]. In order to overcome these deficiencies, a variety of solid acid catalysts have been developed. For instance, they include zeolites [2-5], bentonites [6-8], hetero-polyacids [9-11], metal oxides [12-17], carbon-based solid acids [18,19], and metal organic frameworks [20-23], etc. Currently, many studies have focused on the esterification of n-butanol with acetic acid [22-25]. 12-Tungstophosphoric acid-encapsulated metal-organic framework UiO-66 (30HPW@UiO-66) could be used to catalyze the esterification reaction of acetic acid with n-butanol, which resulted in the conversion of 80.21% at the optimum conditions [22] and HPW@UiO-67 has been studied as catalyst for this reaction, having the conversion of acetic acid above 63.1% after four reaction cycles [23]. The Porous Niobium Oxide (V) catalyst was utilized in the esterification reaction of acetic acid with n-butanol, where a maximum ester yield of 89% was determined at the optimum conditions [24]. The catalyst showed stable activity over five cycles only with a little decrease in yield. $SO_4^{2-}/ZrO_2@Nb_2O_5$-NT catalyst was exploited as a solid acid catalyst for the esterification of acetic acid with n-butanol, in which the esterification rate reached up to 92.31% under the optimum conditions [25]. SO_4^{2-}/M_xO_y metal oxide-based solid acids have the advantages of strong acidity, high catalytic activity, easy separation, low waste generation, good environmental friendliness,

etc. [13]. Among them, two main kinds of sulfated zirconia (SO_4^{2-}/ZrO_2) and sulfated titanium oxide (SO_4^{2-}/TiO_2) have been widely investigated due to their strong acidities in many reactions. However, they have some shortages like rapid deactivation and low service life, which hindered their application in practice [26-30]. For these problems, extensive efforts have been involved in improving the performance of SO_4^{2-}/M_xO_y. The representative schemes involved the partial replacement of M_xO_y with different oxides such as SiO_2, CeO_2 and SnO_2 [12,15-17] or the load of sulfated metal oxide on porous silica materials such as MCM-41 and SBA-15 [26-28,32]. Meanwhile, there are many literatures in which new types of modified SO_4^{2-}/M_xO_y solid acid catalysts have been developed [13,31].

However, there is very little attention to the usage of CeO_2 as the main oxide of SO_4^{2-}/M_xO_y solid acid. Although the CeO_2/SBA-15 catalyst with high specific surface area has been studied, its application is limited mainly to the NH_3-SCR reaction [33]. Since the process of acid treatment to enhance surface acidity was not involved in the preparation of this catalyst, it is not suitable that CeO_2/SBA-15 would be considered the solid acid catalyst for the esterification reaction.

In this paper, a novel solid acid based on ceria and amorphous silica was prepared using ceric sulfate and sodium metasilicate and was characterized by different techniques. Moreover, its catalytic activity was examined for the esterification reaction.

Combination of sulfated ceria and amorphous silica would be able to improve the catalytic activity and stability of the solid acid. First, sulfated ceria can exhibit a strong acidity and reusability. Ceric sulfate as a Lewis acid could become an effective catalyst for the esterification reaction, but it was difficult to use it repeatedly because of the considerable loss of ceric sulfate during the reaction. Conversion of ceric sulfate to

sulfated ceria can enhance the stability and reusability of the solid acid. Second, the utility of inexpensive amorphous silica instead of MCM-41 and SBA-15 gives rise to a considerable increase in the specific surface area of sulfated ceria. Therefore, our solid acid catalyst could have a promising application in the esterification reaction.

2. Materials and Methods

2.1 Catalyst preparation

The materials used for the preparation of solid acids were $Ce(SO_4)_2 \cdot 4H_2O$ (99%, analytical pure), $Na_2SiO_3 \cdot 5H_2O$ (99%, analytical pure), 96wt% H_2SO_4 and 20wt% aqueous ammonia.

Ceria and amorphous silica-based solid acid were obtained as follows: The calculated amount of $Ce(SO_4)_2 \cdot 4H_2O$ was dissolved in 100 mL of a 0.2 mol/L sulfuric acid solution at 5 °C. Dissolving in dilute sulfuric acid solution was to prevent hydrolysis of $Ce(SO_4)_2 \cdot 4H_2O$. Then 42.4 g of $Na_2SiO_3 \cdot 5H_2O$ (SiO_2 0.2 mol) was added to and 300 mL of distilled water in the beaker, which resulted in SiO_2 concentration below 5%. Sodium metasilicate solution was slowly added to ceric sulfate solution under magnetic stirring at 10 °C to form silica and cerium hydroxide (IV) precipitates. The pH of the solution was maintained at 6 by the addition of 0.5 mol/L sulfuric acid or 0.5 mol/L aqueous ammonia. The stirring continued until the formation of a pale yellow precipitate. The reaction mixture was kept undisturbed for 24 h and the precipitate was separated. Then, the precursor obtained when drying the precipitate at 90 °C for 12 h was impregnated in 5.0 mol/L of sulfuric acid solution for 8 h and then filtered, followed by calcination at 600 °C for 2 h. We will adopt S/C-S designation for the obtained solid acid catalyst.

2.2 Esterification reaction

The esterification reaction was carried out in a three-necked flask under atmospheric pressure, which is equipped with a magnetic stirrer, a thermometer and a refluxing condenser tube. The reaction conditions were as follows: the molar ratio of *n*-butanol to acetic acid was 1.6, the catalyst amount was 2.3 wt% (weight percentage of the reaction mixture), the reaction time was 120min and the reaction temperatures were 120 °C. After the reaction, the catalyst was immediately separated from the reaction mixture by filtering. Then, the titration experiment was rapidly performed, which was used to determine the residual acid. Namely, 0.50 mL reaction mixture was added in 20.00 mL absolute alcohol and titrated by 0.10 mol/L NaOH solution using phenolphthalein as an indicator. Then, the conversion of acetic acid was measured using the following equation:

$$\text{The conversion of acetic acid}(\%) = \frac{(M_0 - M_1)}{M_0} \times 100 \qquad \text{(eq.1)}$$

M_0: Acid value before reaction

M_1: Acid value after reaction

In order to examine the stability, prepared solid acid catalyst was repeatedly used for the batch reaction process. After each catalytic examination was completed, the catalyst was filtered from the reaction mixture, and dried at 70 °C for 10 h in air. Then, the catalyst without any further intermediate reactivation was repeatedly used in a new reaction cycle under the same reaction conditions.

2.3 Catalyst characterization

The crystalline structure and phase composition of the prepared solid acids were analyzed by Rigaku Miniflex X-ray diffractometer with a Cu K_α radiation source at 40kV and 100mA, and the XRD patterns were recorded by scanning the samples in a 2θ range of 5-60°, applying a scan speed of 3°/min. The average crystallite size of the product was

estimated with the help of Scherrer equation. A specific surface area of the sample was determined by using N_2 adsorption isotherms at -196 °C by the multipoint Brunauer-Emmett-Teller (BET) method using a Quantachrome Autosorb Automated Gas Sorption system. The surface area was calculated with the BET equation and the pore volume and diameter were calculated by using the BJH method. The morphologies and sizes were observed using a JSM-6610A scanning electron microscope at an accelerating voltage of 20 kV. Acid strength of the samples was determined by titration with n-butylamine using thymol blue (H_0= +1.2), anthraquinone (H_0= -8.20) and *p*-nitrotoluene (H_0= -11.35) as the Hammett indicators and benzene as the solvent. The titration was carried out by dispersing 0.10 g of catalyst in 5 mL of dry benzene; two indicator drops in benzene solution were then added to the resulting dispersed solution and the titration was done with a solution of n-butylamine (0.01N). The acidity strength was expressed in terms of the Hammett acidity (H_o). Fourier transform infrared (FT-IR) spectra of the prepared solid acid and product were recorded on a Nicolet 6700 IR spectrometer at 4 cm^{-1} resolution in the spectral range of 4000-500 cm^{-1} using the conventional KBr pellet technique. FT-IR of adsorbed pyridine spectra was recorded on a Frontier FT-IR spectrometer. Before measurement, the sample was pretreated at 300 °C for 1 h in a vacuum followed by being cooled to 30 °C and adsorbed pyridine vapor for 0.5 h. The adsorbed pyridine was subsequently degassed for 1 h at 150 °C and removed. Then, the FT-IR spectrum of the adsorbed pyridine was recorded. Thermogravimetric analysis (TGA)/differential thermal analysis (DTA) of samples was carried out using the instrument Shimadzu TGA-5H and Shimadzu DTA-50. The sample was placed in a platinum container and TGA was carried at a ramping rate of 20 °C/min with the sample gas as Nitrogen at a flow rate of 60.0 ml/ min up to 950 °C. The sample was decomposed

by combustion and all the sulfur species were converted into SO_3. The formed SO_3 was absorbed in calcium iodide solution and the sulfur content was determined by titration.

3. Results and Discussion

3.1 Characterization of the prepared solid acid

3.1.1 XRD analysis

The XRD pattern of the prepared S/C-S solid acid is shown in Fig. 1. The strong characteristic peaks at 2θ values of 27-29°, 32-34°, 47-49°, 56-58° are assigned to ceria.

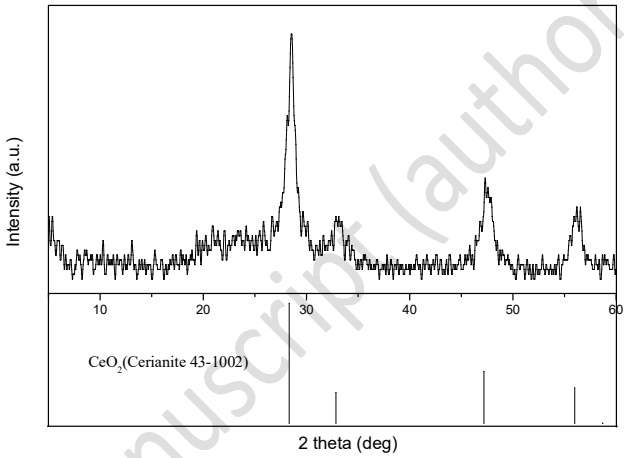

Figure 1. XRD pattern of S/C-S solid acid with 40 wt% ceria sulfate loading obtained after calcinations at 600 °C for 2 h

As indicated in Fig. 1, the peaks corresponding to CeO_2 were observed in the diffraction pattern of the solid acid, which is consistent with the standard database of Cerianite (PDF43-1002). No crystalline phases of impurities were found in the diffraction patterns, but the crystallization was not completed enough. The absence of the diffraction peaks corresponding to silica indicates the presence of amorphous silica.

The broad diffraction peaks of CeO_2 elucidate particles being of the little size.

By using the Scherrer equation (eq.2), the average crystallite size of the prepared solid acid at various peak positions was 12.7 nm.

$$D_C = \frac{K\lambda}{\beta cos\theta} \qquad \text{(eq.2)}$$

The definitions of the equations' symbols are as follows: The full width at half maximum (FWHM) in radians = β, the degree of diffraction angle = θ, the crystallite size = Dc, X-ray wavelength=λ, the shape factor is equal to Scherrer's constant, K = 0.94.

The small crystallite size shows that coordinated SO_4^{2-} on the surface of CeO_2 suppressed the crystal growth. This allows the particles of the prepared solid acid to get further smaller size and the specific surface area to be increased, which is advantageous to increasing the activity of solid acid catalyst.

3.1.2 The surface morphology analysis

SEM images of the prepared S/C-S solid acid are shown in Fig. 3. As shown in Fig. 2, the size and shape of the particles are similar, and the particle size ranges from 100 to 300 nm. A mass of small pieces is formed and has pores inside. This means that the obtained solid acid may have a relatively large specific surface area.

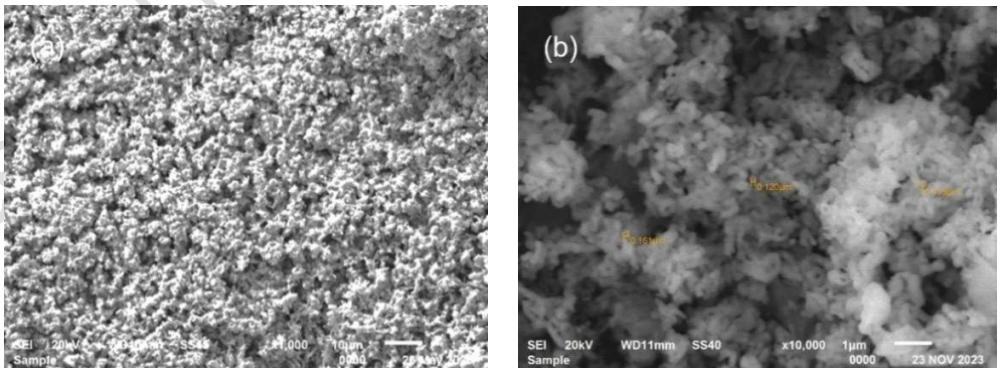

Figure 2. SEM images of S/C-S solid acid with 40 wt% ceria sulfate loading obtained after calcinations at 600 °C for 2 h ((a) 1000 times and (b) 10,000 times)

3.1.3 BET specific surface area

The N_2 adsorption isotherm of S/C-S solid acid is shown in fig.3. The isotherm belongs to type IV and the solid acid still maintains the mesoporosity structure after calcination of 600 °C.

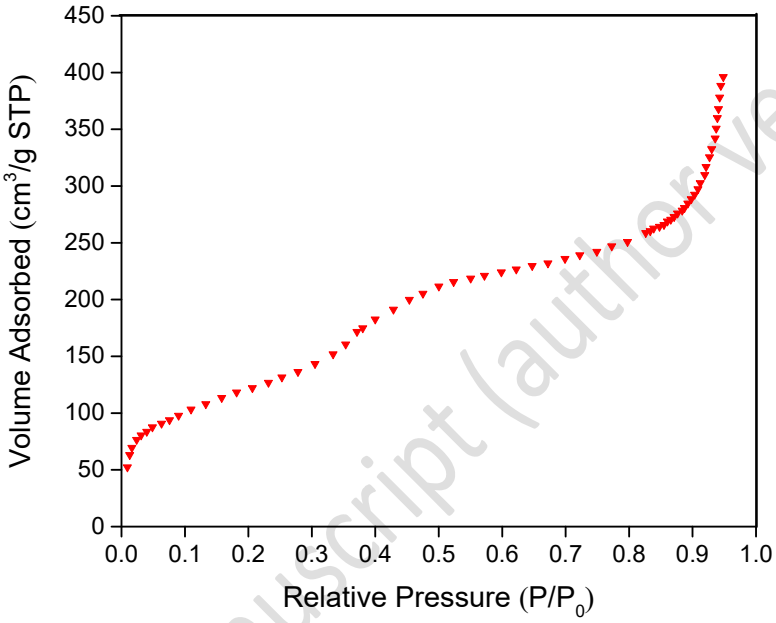

Figure 3. Nitrogen adsorption isotherm of S/C-S solid acid with 40 wt% ceria sulfate loading obtained after calcinations at 600 °C for 2 h

The BET specific surface area, pore volume and pore diameter of S/C-S solid acid are reported in Table 1.

Table 1. Surface area and porosity properties of S/C-S solid acid

sample	BET specific surface area / $m^2 \cdot g^{-1}$	BJH cumulative pore volume / $cm^3 \cdot g^{-1}$	BJH average pore diameter / nm
S/C-S	440	0.52	5.61

The specific surface area of the solid acid is 440 m^2/g, which is comparable to that of CeO_2/SBA-15 catalyst for NH_3-SCR reaction [33]. It is shown that amorphous silica can provide a specific surface area of the solid acid more than 400 m^2/g. Also, pore volume and pore size data show that sulfated ceria/amorphous silica solid acid is a mesoporous material. The fact that the prepared solid acid catalyst has a large specific surface area and is a porous material is beneficial to improve the catalytic activity.

3.1.4 Acidity strength

The acid strength of the catalyst was determined by Hammett indicator method, and the results are listed in Table 2. In this table, (+) indicates that the color of the base form has been changed to that of the conjugated acid form, while (-) means that there is no color change. S/C-S solid acid exhibited obvious color change corresponding to thymol blue and anthraquinone indicators, but no color change for *p*-nitrotoluene.

Table 2. Acidity of solid acid with Hammett indicators

sample	thymol blue	anthraquinone	*p*-nitrotoluene
S/C-S	+	+	-

As can be seen from Table 2, the two indicators except *p*-nitrotoluene exhibited obvious color change. Thus, the prepared solid acid has at least the acidity of $-11.35<H_0<-8.2$

3.1.5 Acid sites structure

The infrared absorption spectrum of the prepared S/C-S is shown in Fig. 4.

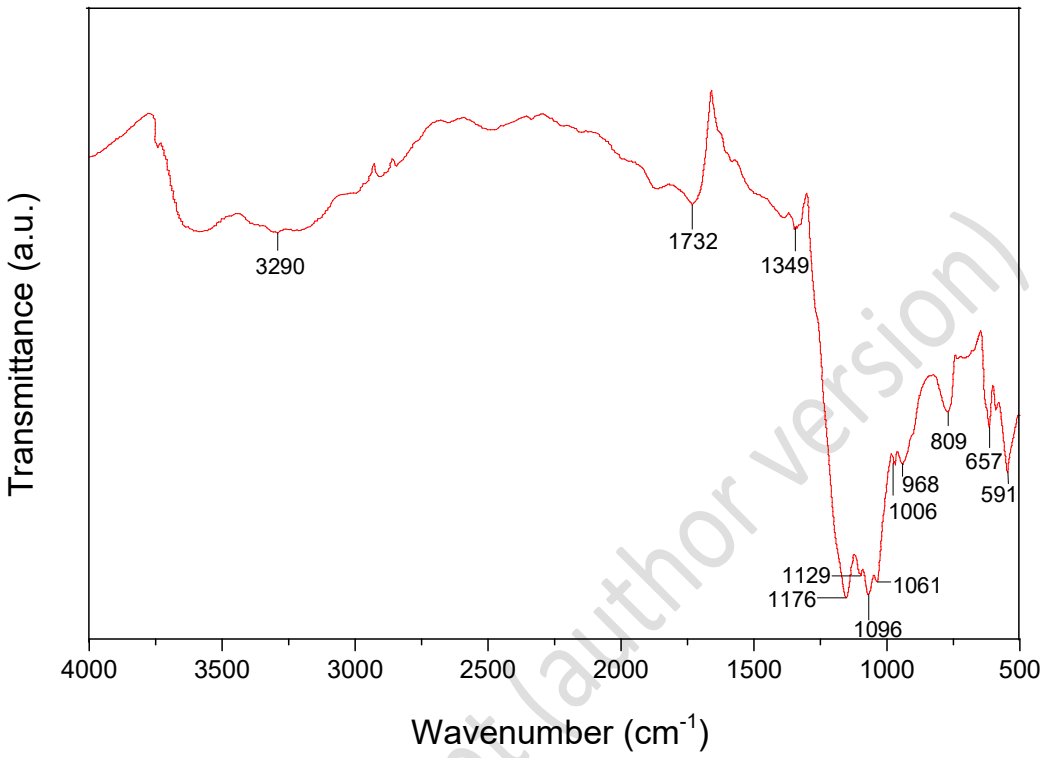

Fig.4 IR spectra of S/C-S solid acid with 40 wt% ceria sulfate loading obtained after calcinations at 600 °C for 2 h

As can be seen in Fig. 4, the band located at 3290 cm^{-1} corresponds to the stretching vibration of -OH, which is related to some adsorbed water of solid acid, and the band in the region of 809, 657 and 591 cm^{-1} corresponds to Ce-O bonds of ceria. The bands at 1732, 1176 and 1096 cm^{-1} correspond to the Si-O-Si bonds of silica and the absorption area at 968 cm^{-1} is attributed to -OH stretching vibration of Si-OH groups. According to the previous researches, the significant absorption band of the bidentate anion in SO_4^{2-}/M_xO_y solid acid is observed in the region of 980~1230 cm^{-1} [34] and 957~1243 cm^{-1} [35]. Therefore, the absorption bands at 1006, 1061 and 1129 cm^{-1} can be attributed to the bidentate coordinated sulfate ions.

The characteristic bands at 1006 and 1129 cm^{-1} is attributed to the symmetric stretching vibration of the O=S=O bond in the structure of the bidentate sulfate ion, and the characteristic bands at 1061 cm^{-1} are attributed to the asymmetric stretching vibration of the O=S=O bond. Such a bidentate structure seems to account for many acidic sites on surface of sulfated metal oxides, causing the sample possess acidity [13]. From the IR spectra of the prepared solid acid, it can be seen that SO_4^{2-} is coordinated to ceria in the form of O=S=O bonds on the surface of the solid acid, which is the significant reason for the formation of the active acid centre on the surface of S/C-S solid acid.

3.1.6 Types of acids

The pyridine absorbed to the prepared S/C-S was used to determine Brønsted and Lewis acid sites. The FTIR-pyridine adsorption spectra of the S/C-S solid acid are shown in Fig. 5. As pointed out in fig. 5, significant peaks exist in the area of 1450 and 1600 cm^{-1}. The pyridinium ions (PyH^+) formed by the transfer of protons from the acidic hydroxyl groups in the solid acid to the organic base [34]. The band at 1450 cm^{-1} is assigned to the adsorption of coordinated pyridine in Lewis sites and wide bands from 1600 to 1640 cm^{-1} correspond to Brønsted acid sites. Fig. 5 shows that the transmittance of the Lewis acid site is stronger than that of the Brønsted acid site. This indicates the presence of Lewis acid sites on the surface of the catalyst is more dominant.

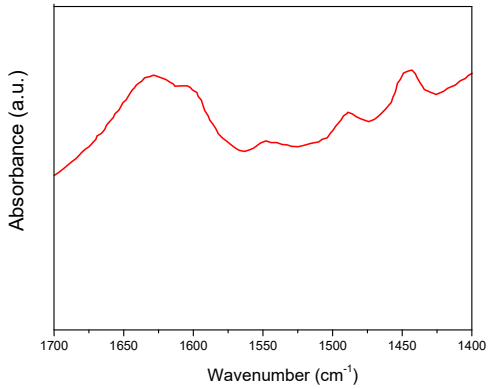

Fig. 5 Pyridine adsorption FT-IR spectra of S/C-S solid acid with 40 wt% ceria sulfate loading obtained after calcinations at 600 °C for 2 h

3.1.7 The content analysis of coordinated SO_4^{2-} on the solid acid surface

Thermogravimetric profile of the prepared solid acid was shown in Fig. 6. TG profiles of solid acids show several weight losses. The weight loss in the range of 21-205 °C causes by the adsorbed water of the solid acid, and the weight loss between 205 °C and 422 °C is observed because of some bound water. It can also be seen that weight loss of 2.484 wt% caused ranging from 422 °C to 846 °C corresponds to the thermal decomposition of the remained $Ce(OH)_4$, silanol groups of silica, a little of sulfated ceria. This phenomenon may be attributed to the fact that a significant weight loss in the range of 422 °C ~ 846 °C must be expected, yet there is only weight loss of 2.484 wt% if SO_4^{2-} in the calcined solid acid exists mostly as the form of $Ce(SO_4)_2$. This indicates that SO_4^{2-} may be bound to the surface of CeO_2. The sulfur-containing components on surface of the solid acid were lost relatively gradually in the region of 422 °C ~ 846 °C and then lost rapidly beyond this temperature range. The weight loss of 6.806 wt% in the temperature range from 846 to 983 °C corresponds to the decomposition of sulfated ceria. The thermogravimetric analysis displays that SO_4^{2-} content coordinated to the prepared solid acid is considered as

more than 7 wt%. From this result, it is proved that the obtained S/C-S exhibits low losses of sulfur-containing components at temperatures below 400 °C, and the SO_4^{2-} coordinate bond on the solid acid surface is stable, so that it is not easily lost during the reaction.

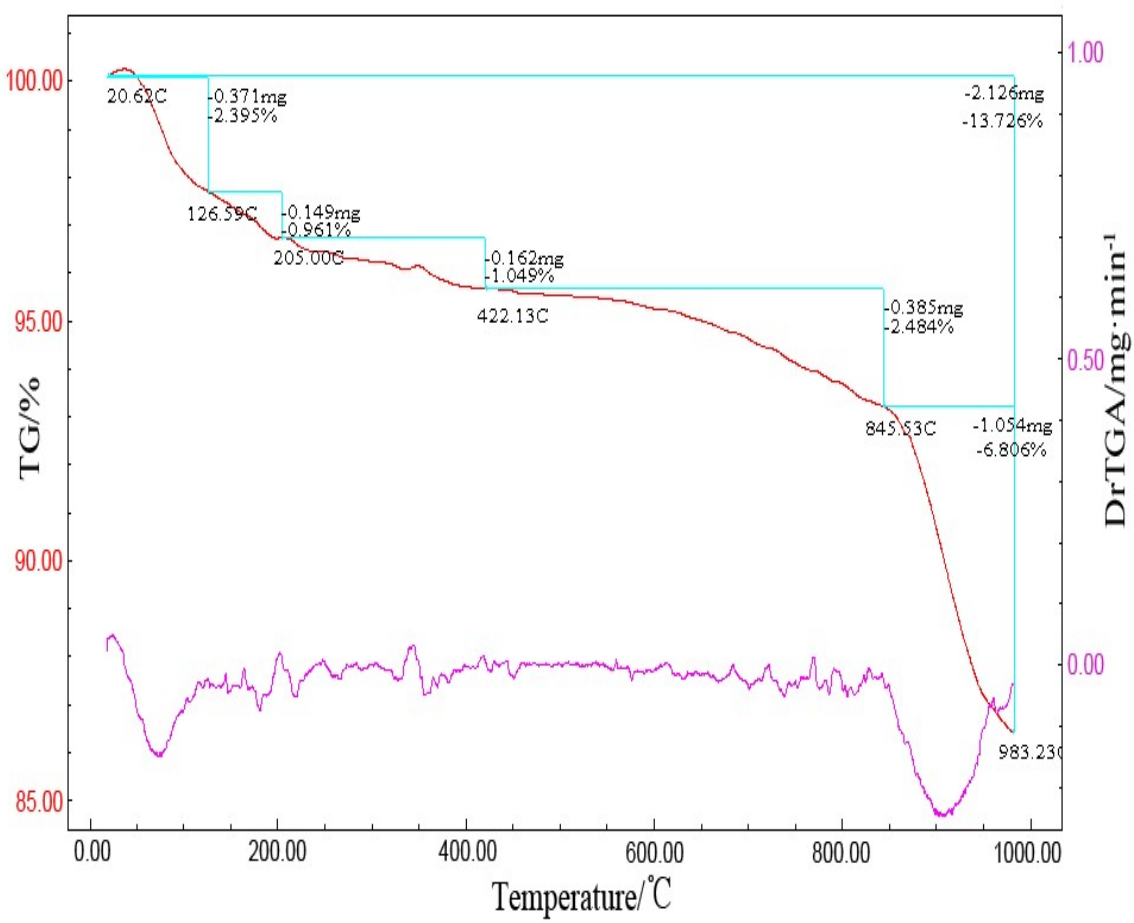

Fig. 6 TG profiles of S/C-S solid acid with 40 wt% ceria sulfate loading obtained after calcinations at 600 °C for 2 h

3.2 Optimization of esterification conditions

The main factors on the conversion of acetic acid are molar ratio of *n*-butanol to acetic acid, the catalyst amount, reaction time, reaction temperature.

3.2.1 Effect of molar ratio of n-butanol to acetic acid on catalytic activities

Fig. 7 shows the effects of the molar ratio of n-butanol to acetic acid on the esterification efficiency of S/C-S solid acid. It can be observed that the conversion of acetic acid increases from 76.1 to the maximum 92.4% as the molar ratio of n-butanol to acetic acid increases from 0.7 to 1.6. Because an excess of n-butanol is normally used to allow the equilibrium to move into the production of butyl acetate. When the molar ratio of *n*-butanol to acetic acid exceeds 1.6, there is a decrease in the conversion of acetic acid. A high molar ratio of n-butanol to acetic acid may dilute the concentration of acidity and slow down the reaction. Thereby, the molar ratio of 1.6 is enough suitable to achieve a high yield.

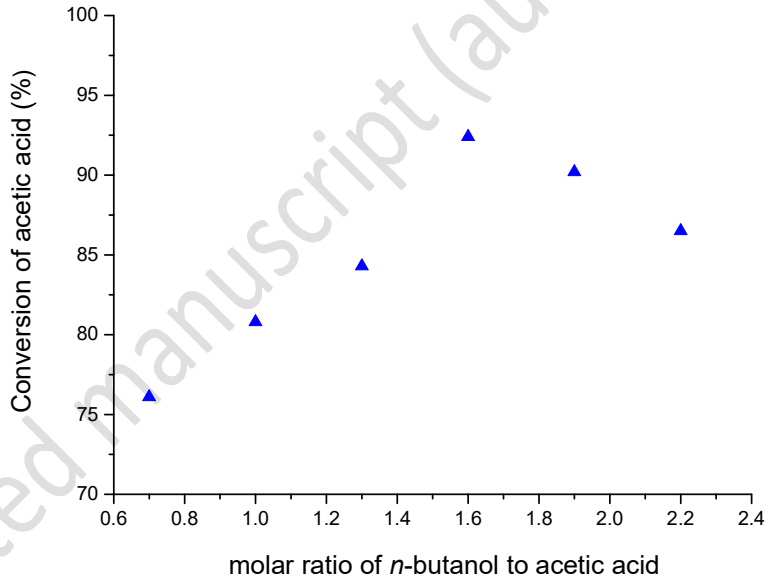

Fig. 7 Effect of molar ratio of *n*-butanol to acetic acid on conversion of acetic acid (Reaction conditions: catalyst amount 3 wt%, reaction time 150 min, and reaction temperature 120 °C)

3.2.2 Effect of catalyst amount on catalytic activities

The reaction of butyl acetate synthesis is influenced strongly by the catalyst and the time to reach equilibrium depends on the type and catalyst amount. The variation of conversion of acetic acid with catalyst amount is shown in Fig.8. As can be seen in Fig.8, with the increase of catalyst amount, the conversion of acetic acid increases and then tends to decrease slightly from more than 2.3 wt%. This is attributed to the fact that the higher catalyst loading increases the loss of the product adsorbed on the catalyst during the separation of the product and S/C-S solid acid. Hence, a reasonable catalyst amount of 2.3 wt% was chosen.

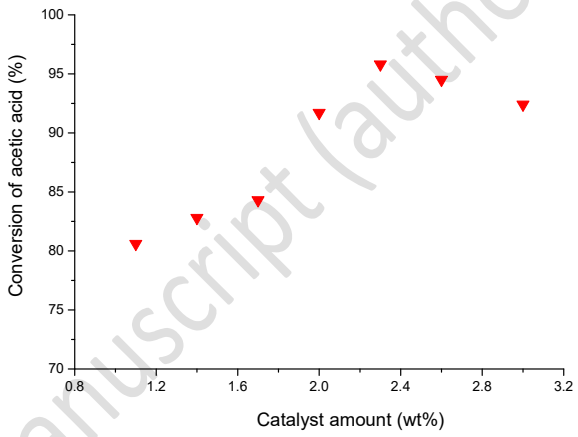

Fig. 8 Effect of catalyst amount on conversion of acetic acid (Reaction conditions: molar ratio of n-butanol to acetic acid 1.6, reaction time 150 min, and reaction temperature 120 °C)

3.2.3 Effect of reaction time on catalytic activities

The conversion variation of acetic acid with reaction time is shown in Fig. 9. As shown in Fig. 9, with the increase of reaction time, the yield increases and then reaches a maximum at 120 min, and then decreases slightly. This indicates that when the reaction time is 120 min, the esterification reaction gets to the equilibrium of the main phase and the

conversion of acetic acid reaches a maximum. Hence, a reasonable reaction time of 120 min was chosen.

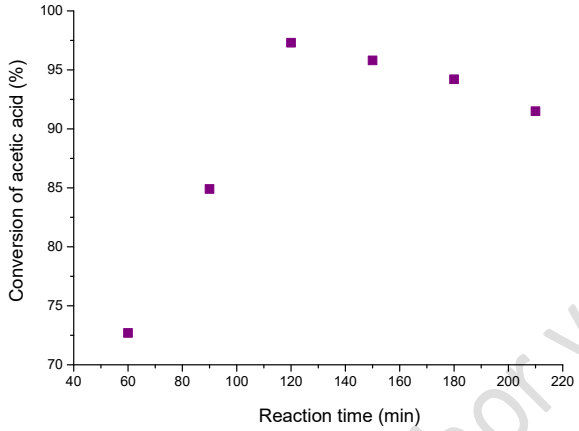

Fig. 9 Effect of reaction time on conversion of acetic acid (Reaction conditions: molar ratio of n-butanol to acetic acid 1.6, catalyst amount 2.3 wt%, and reaction temperature 120 °C)

3.2.4 Effect of reaction temperature on catalytic activities

The conversion variation of acetic acid with reaction temperature is shown in Fig. 10. As can be seen in Fig. 10, with the increase of reaction temperature, the conversion of acetic acid increases and reaches a maximum at 120 °C, and then decreases. The reason for the decrease in conversion at reaction temperatures above 120 °C is that the higher the reaction temperature, the higher the amount of butanol dissolves in water and is lost.

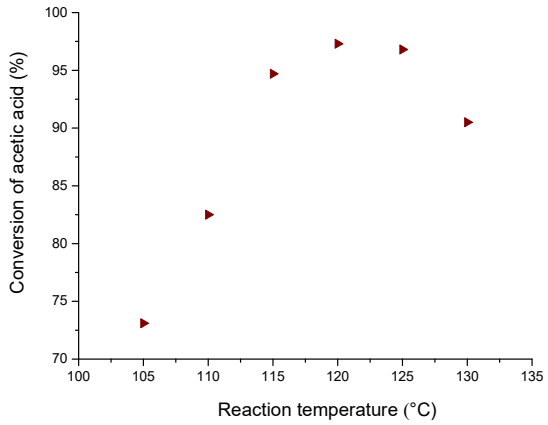

Fig. 10 Effect of reaction temperature on conversion of acetic acid (Reaction conditions: molar ratio of n-butanol to acetic acid 1.6, catalyst amount 2.3 wt%, and reaction time 120 min)

Eventually, the optimum conditions for the synthesis of butyl acetate were as follows: the molar ratio of *n*-butanol to acetic acid was 1.6, the catalyst amount was 2.3 wt%, the reaction time was 120 °C and then the reaction time was 120 min. At these conditions, the conversion of acetic acid was 97.3%.

The catalytic activity of S/C-S solid acid compared to the other heterogeneous catalysts, as shown in Table 3. In the concept of optimum reaction condition, a lower molar ratio of *n*-butanol to acetic acid and shorter reaction time than those of other catalysts were obtained. Also, the catalyst amount was about 2.3%, which was a relatively low value than that of other catalysts. The conversion of acetic acid at the optimum reaction conditions was 97.3%, higher than the 30 HPW@UiO-66 and $SO_4^{2-}/ZrO_2@Nb_2O_5$-NT catalysts.

Table 3 shows that the prepared catalyst has a relatively high catalytic activity compared to the other catalysts under the optimum conditions.

Table 3 Comparison of S/C-S with other heterogeneous catalysts for the esterification of n-butanol with acetic acid

Catalyst	Reaction condition				Conversion of acetic acid /%	Reference
	n-butanol to acetic acid molar ratio	Catalyst amount / wt%	Temperature/ °C	Time/ h		
S/C-S	1.6	2.3	120	2	97.3	
30HPW@UiO-66	2.0	3.0	120	3	80.2	[22]
SO_4^{2-} /ZrO_2@Nb_2O_5-NT	2.7	11	118	7	92.31	[25]
$S_2O_8^{2-}$/Al-2.5 wt%Ce–Zn–O	3.0	1.55	115-118	3	98.71	[31]

3.3 Selectivity and reusability of S/C-S solid acid

Fig. 11 shows the IR spectra of the crude products obtained at 120 °C, 140 °C and 160 °C. At 120 °C, the absorption peaks at 2961 and 2875 cm^{-1} correspond to the stretching vibration of two -CH_3, and the absorption peak at 2936 cm^{-1} is assigned to the stretching vibration of -CH_2-. The product butyl acetate is confirmed at wave number 1743 cm^{-1}. According to Fig. 11, a strong peak was observed at 1743 cm^{-1} which indicated the presence of ester-carbonyl group(C=O). Also, the peak of C-O stretching vibrations was observed at 1241 cm^{-1}. The IR spectrum of the product at 120 °C coincides with the standard spectrum of *n*-butyl acetate. The IR spectra of the products at 140 °C and 160 °C contain the bands at 3542 cm^{-1} and 2165 cm^{-1}, which correspond to water, besides the

characteristic absorption bands of *n*-butyl acetate. Therefore, the reaction products were found to be *n*-butyl acetate and a small amount of water. The absence of characteristic bands relating to ether (1070-1150 cm^{-1}) and alkene (1650 cm^{-1}) means that there are no other side products in addition to *n*-butyl acetate, which displays that the prepared solid acid is a highly selective catalyst.

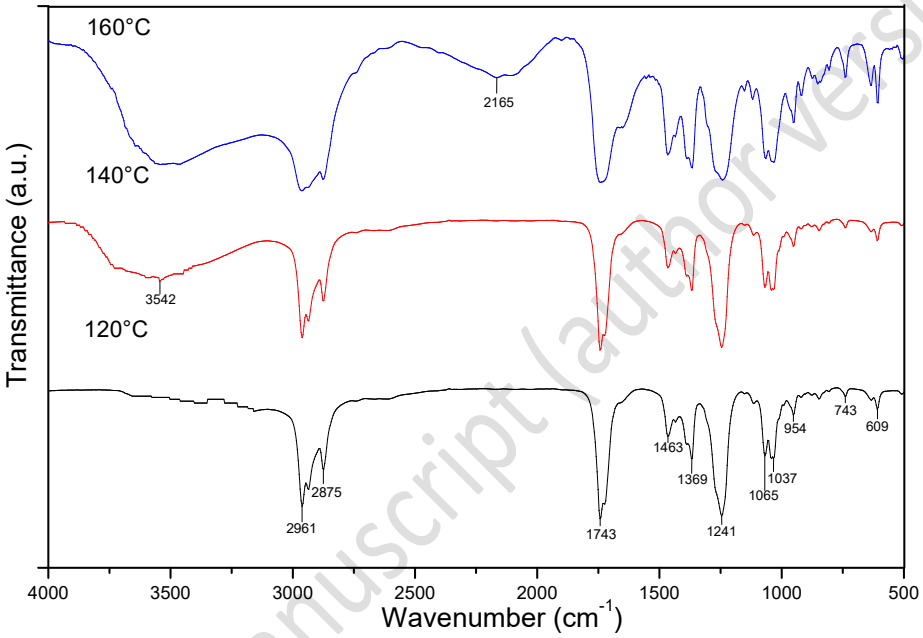

Fig. 11 IR spectra of the synthesized reaction product at various esterification temperatures (Reaction conditions: molar ratio of n-butanol to acetic acid 1.6, catalyst amount 2.3 wt%, and reaction time 120 min)

To examine the reusability of the S/C-S solid acid catalyst, the conversion of acetic acid was measured in the esterification reaction for five runs. The data of the reusability under the optimum synthesis conditions are shown in Fig. 12.

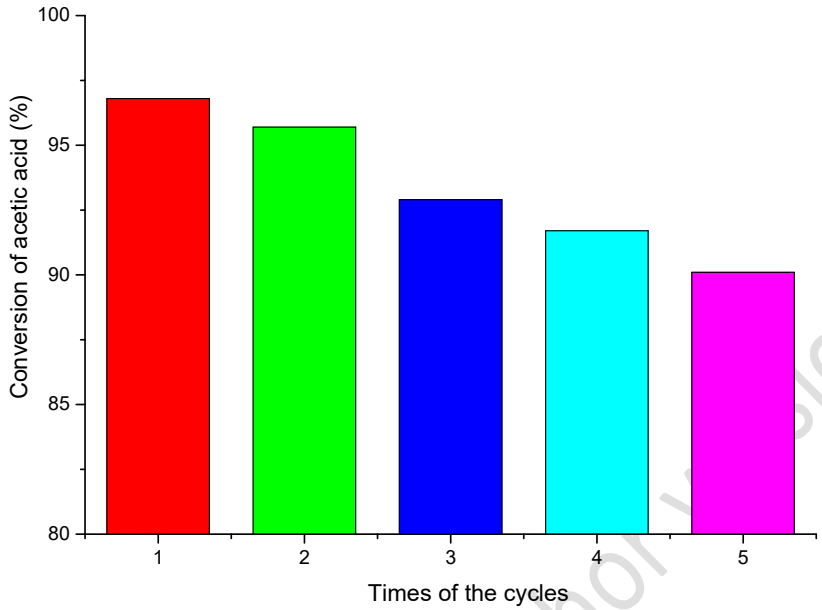

Fig. 12 Conversion of acetic acid with the times of the cycles (Reaction conditions: molar ratio of n-butanol to acetic acid 1.6, catalyst amount 2.3 wt%, reaction temperature 120 °C and reaction time 120 min)

As shown in Fig. 12, the conversion of acetic acid declined slightly in each cycle, but the conversion still reached over 90% for five cycles of S/C-S solid acid. It is well known that loss of sulfur species as well as carbon deposition accounts for the deactivation of SO_4^{2-}/M_xO_y solid acid catalysts.

FT-IR analysis was performed to confirm the deactivation of S/C-S due to acid site blockage by carbon species. Figure 13 shows the IR spectra in the range of 500–4000 cm^{-1} for the reused S/C-S of the first run and the fifth run. The absence of strong peaks at 1600–1800 cm^{-1} indicated that carbonaceous materials were not present on the surface of the S/C-S.

After five cycles, the color of S/C-S surface didn't get dark, meaning that surface coking didn't take place during the reaction.

In order to verify the loss of the sulfur in the catalyst, the sulfur contents of the fresh and used S/C-S solid acids were measured, as shown in Table 4. It was found that when the catalyst was repeatedly applied for five cycles, the sulfur content decreased slightly from 2.88 wt% in the fresh catalyst to 2.57 wt% in the used catalyst. This means that the less leaching of the sulphonic groups into the reaction medium by solvation occurred.

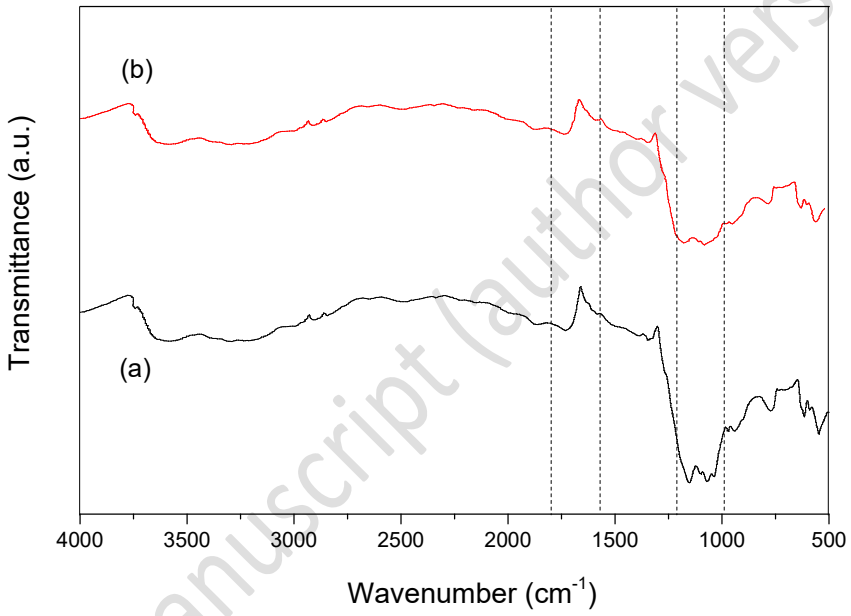

Fig. 13 IR spectra of S/C-S solid acids for different repeated reaction runs: *a* first use, *b* fifth use

Table 4. Conversion of acetic acid over the fresh and used S/C-S solid acids and their sulfur content

Item	Fresh S/C-S	Used S/C-S (after fifth recycling)
Conversion of acetic acid /%	97.3	2.88

Sulfur content wt%	90.2	2.56

The high catalytic activity even in the final cycle confirms that S/C-S solid acid has excellent stability.

However, if the conversion was decreased to less than 80% with the cycles, the catalyst should be regenerated. Concentrated sulfuric acid could be available for the regeneration of the deactivated catalyst.

4. Conclusion

In this paper, we prepared and characterized a novel solid acid catalyst based on ceria and amorphous silica. The results of experiments show that the prepared solid acid can be used as an effective catalyst for the esterification reaction. The various instrumentations including XRD, N_2 sorption, SEM, Hammett Indicator titration, FT-IR, TG-DTA analysis indicated that that the obtained catalyst was composed of CeO_2 and amorphous silica and exhibited the acidity by sulfated ceria. Under the optimum reaction conditions, the highest conversion of acetic acid was observed as 97.3%. When the prepared solid acid was used in the synthesis reaction of butyl acetate, no any side-products such as ether or alkene were formed even at temperatures higher than the optimum reaction temperature, and the conversion of acetic acid reached above 90% for five cycles. It means that sulfated ceria and amorphous silica solid acid catalyst has good selectivity and reusability, which has potential applications for many reactions catalyzed with any other acids.

Geolocation information: Faculty of Chemistry, **Kim Il Sung** University.

Ryongnam-Dong, Taesong District, Pyongyang, Democratic People's Republic of Korea.

Declaration of interest: The authors report no conflicts of interest.

Funding: This research did not receive any specific grant from funding agencies in the public, commercial, or not-for-profit sectors.

Data Availability Statement:

This data is available from the authors upon reasonable request.

The data that support the findings of this study are available from the corresponding author, upon reasonable request.

Author contributions:

Kum-Hyok Song designed and performed the experiments, analysed the results.

Un-Ha Kim prepared figures and wrote the manuscript.

Myong Yun and Se-Ok Pak supervised (revised and edit).

References

[1] H. Pan, Q. Xia, Y. Wang, Z. Shen, H. Huang, Z. Ge, X. Li, J. He, X. Wang, L. Li, Y. Wang, Recent advances in biodiesel production using functional carbon materials as acid/base catalysts, *Fuel Process. Technol.* **237** (2022) 107421. https://doi.org/10.1016/j.fuproc.2022.107421

[2] N. S. Lani, N. Ngadi, I. Mohammed Inuwa, L. Anako Opotu, Z. Y. Zakaria, S. Haron, A cleaner approach with magnetically assisted reactor setup over CaO-zeolite/Fe_3O_4 catalyst in biodiesel production: evaluation of catalytic performance, reusability and life cycle assessment studies, *J. Clean. Prod.* **419** (2023) 138329. https://doi.org/10.1016/j.jclepro.2023.138329

[3] W. B. Widayatno, G. Guan, J. Rizkiana, X. Du, X. Hao, Z. Zhang, Selective catalytic conversion of bio-oil over high-silica zeolites, *Bioresour. Technol.* **179** (2015) 518-523. http://dx.doi.org/10.1016/j.biortech.2014.12.046

[4] J. Yu, J. Luo, Y. Zhang, J. Cao, C.-C. Chang, R. J. Gorte, W. Fan, An examination of alkali-exchanged BEA zeolites as possible Lewis-acid catalysts, *Microporous Mesoporous Mater.* **225** (2016) 472-481. http://dx.doi.org/10.1016/j.micromeso.2016.01.039

[5] V. S. Marakatti, A. B. Halgeri, G. V. Shanbhag, Metal ion-exchanged zeolites as solid acid catalysts for the green synthesis of nopol from Prins reaction, *Catal. Sci. Technol.* **4** (2014) 4065-4074. https://doi.org/10.1039/c4cy00596a

[6] N. Rinaldi, N. D. E. Purba, A. Kristiani, E. Agustian, R. R. Widjaya, A. A. Dwiatmoko, Bentonite pillarization using sonication in a solid acid catalyst preparation for the oleic acid esterification reaction, *Catal. Commun.* **174** (2023) 106598. https://doi.org/10.1016/j.catcom.2022.106598

[7] H. Rahimzadeh, M. Tabatabaei, M. Aghbashlo, H. K. S. Panahi, A. Rashidi, S. A. H. Goli, M. Mostafaei, M. Ardjmand, A. S. Nizami, Potential of acid-activated bentonite and SO_3H-functionalized MWCNTs for biodiesel production from residual olive oil under biorefinery scheme, *Front. Energy Res.* **6** (2018) 1–10. https://doi.org/10.3389/fenrg.2018.00137

[8] G. Nagendrappa, R. R. Chowreddy, Organic Reactions Using Clay and Clay-Supported Catalysts: A Survey of Recent Literature, *Catal. Surv. Asia* **25** (2021). https://doi.org/10.1007/s10563-021-09333-9

[9] X. Guo, F. Guo, Y. Li, Z. Zheng, Z. Xing, Z. Zhu, T. Liu, X. Zhang, Y. Jin, Dehydration of D-xylose into furfural over bimetallic salts of heteropolyacid in

DMSO/H_2O mixture, *Appl. Catal. A* **558** (2018) 18–25. https://doi.org/10.1016/j.apcata.2018.03.027

[10] F. Huang, Y. Su, Y. Tao, W. Sun, W. Wang, Preparation of 5-hydroxymethylfurfural from glucose catalyzed by silica supported phosphotungstic acid heterogeneous catalyst, *Fuel* **226** (2018) 417-422. https://doi.org/10.1016/j.fuel.2018.03.193

[11] X. Cao, J. Ren, C. Xu, K. Zhang, J. Lan, Preparation, Characterization of Dawson-type Heteropoly Acid Cerium (III) Salt and Its Catalytic Performance on the Synthesis of n-Butyl Acetate, *Chin. J. Chem. Eng.* **21** (2013) 500-506. https://doi.org/10.1016/S1004-9541(13)60493-0

[12] S. M. Ibrahim, A. Mustafa, Synthesis and characterization of new bifunctional SnZrSi oxide catalysts for biodiesel production, *J. Mol. Liq.* **354** (2022) 118811. https://doi.org/10.1016/j.molliq.2022.118811

[13] J. Wang, H. Pan, A. Wang, X. Tian, X. Wu, Y. Wang, Synthesis and characterization of $S_2O_8^{2-}$/ZnFex$Al_{2-x}O_4$ solid acid catalysts for the esterification of acetic acid with n-butanol, *Catal. Commun.* **62** (2015) 29-33. http://dx.doi.org/10.1016/j.catcom.2015.01.009

[14] F. Yang, Y. Li, Q. Zhang, X. F. Sun, H. X. Fan, N. Xu, Selective conversion of cotton cellulose to glucose and 5-hydroxymethyl furfural with SO_4^{2-}/MxOy solid superacid catalyst, *Carbohydr. Polym.* **131** (2015) 9-14. http://dx.doi.org/10.1016/j.carbpol.2015.05.036

[15] X. Li, S. Ren, L. Liu, X. Xing, L. Chen, J. Li, J. Yang, Q. Liu, Superior PbO-resistance of CeO_2/ZrO_2 catalyst promoted by solid superacid SO_4^{2-}/ZrO_2 for

selective catalytic reduction of NOx with NH_3, *Fuel* **332** (2023) 126103. https://doi.org/10.1016/j.fuel.2022.126103

[16] S. Cai, T. Xu, P. Wang, L. Han, S. Impeng, Y. Li, Self-protected CeO_2-SnO_2@SO_4^{2-}/TiO_2 catalysts with extraordinary resistance to alkali and heavy metals for NOx reduction, *Environ. Sci. Technol.* **54** (2020) 12752–12760. https://doi.org/10.1021/acs.est.0c04911

[17] Z. Han, X. Li, X. Wang, Y. Gao, S. Yang, L. Song, Insight into the promoting effect of support pretreatment with sulfate acid on selective catalytic reduction performance of CeO_2/ZrO_2 catalysts, *J. Colloid Interface Sci.* **608** (2022) 2718–2729. https://doi.org/10.1016/j.jcis.2021.10.191

[18] B. Zheng, L. Chen, L. He, H. Wang, H. Li, H. Zhang, S. Yang, Facile synthesis of chitosan-derived sulfonated solid acid catalysts for realizing highly effective production of biodiesel, *Ind. Crops Prod.* **210** (2024) 118058. https://doi.org/10.1016/j.indcrop.2024.118058

[19] Z. Xu, G. Zhang, K. Wang, Efficient conversion of biomass derivatives to furfural with a novel carbon-based solid acid catalyst, *Catal. Commun.* **175** (2023) 106608. https://doi.org/10.1016/j.catcom.2023.106608

[20] Y. Mao, J. Cheng, H. Guo, Y. Shao, L. Qian, W. Yang, Sulfamic acid–modified zeolitic imidazolate framework (ZIF-90) with synergetic Lewis and Brønsted acid sites for microalgal biodiesel production, *Fuel* **331** (2023) 125795. https://doi.org/10.1016/j.fuel.2022.125795

[21] T. Ma, C. Xu, C. Song, W. Li, G. Chen, Z. Yun, J. Qian, Sulfated zirconium metal-organic frameworks as highly efficient catalysts for the green synthesis of n-

amyl acetate, *Sustain. Chem. Pharm.* **43** (2025) 101919. https://doi.org/10.1016/j.scp.2025.101919

[22] T. Ma, D. Liu, Z. Liu, J. Xu, Y. Dong, G. Chen, Z. Yun, 12-Tungstophosphoric acid-encapsulated metal-organic framework UiO-66: A promising catalyst for the esterification of acetic acid with n-butanol, *J. Taiwan Inst. Chem. Eng.* **133** (2022) 104277. https://doi.org/10.1016/j.jtice.2022.104277

[23] T. Ma, C. Song, H. Chen, M. Yin, C. Su, N. Guo, Y. Yao, M. Yu, Y. Wang, G. Chen, Z. Yun, Green catalysis for the production of n-butyl acetate over phosphotungstic acid-encapsulated metal-organic framework UiO-67 catalyst: Catalyst preparation, characterization and reaction kinetics, *Sustain. Chem. Pharm.* **37** (2024) 101389. https://doi.org/10.1016/j.scp.2023.101389

[24] B. Viswanadham, J. Pedada, N. Mameda, B. Putrakumar, Enhanced Catalytic Activity and Reusability of Porous Niobium Oxide for Esterification of Acetic Acid With Butanol, *J. Chem.* (2025). https://onlinelibrary.wiley.com/doi/10.1155/joch/8896509

[25] L. Hu, Y. Liu, M. Liu, P. Zhang, H. Cui, J. He, Enhanced esterification performance by SO_4^{2-}/ZrO_2 anchored Nb_2O_5 nanotube, *J. Ind. Eng. Chem.* **129** (2023) 321-330. https://doi.org/10.1016/j.jiec.2023.08.046

[26] C. L. Chen, S. Cheng, H. P. Lin, S. T. Wong, C. Y. Mou, Sulfated zirconia catalyst supported on MCM-41 mesoporous molecular sieve, *Appl. Catal. A* **215** (2001) 21-30. https://doi.org/10.1016/S0926-860X(01)00504-X

[27] Q. H. Xia, K. Hidajat, S. Kawi, Effect of ZrO_2 loading on the structure, acidity, and catalytic activity of the SO_4^{2-}/ZrO_2/MCM-41 acid catalyst, *J. Catal.* **205** (2002) 318-331. https://doi.org/10.1006/jcat.2001.3424

[28] T. Lei, J. S. Xu, Y. Tang, W. M. Hua, Z. Gao, New solid superacid catalysts for n-butane isomerization: γ-Al_2O_3 or SiO_2 supported sulfated zirconia, *Appl. Catal. A* **192** (2000) 181-188. https://doi.org/10.1016/S0926-860X(99)00404-4

[29] Y. Wang, Y. Gan, R. Whiting, G. Lu, Synthesis of sulfated titania supported on mesoporous silica using direct impregnation and its application in esterification of acetic acid and n-butanol, *J. Solid State Chem.* **182** (2009) 2530-2534. https://doi.org/10.1016/j.jssc.2009.07.003

[30] B. M. Reddy, P. M. Sreekanth, P. Lakshmanan, Sulfated zirconia as an efficient catalyst for organic synthesis and transformation reactions, *J. Mol. Catal. A* **237** (2005) 93-100. https://doi.org/10.1016/j.molcata.2005.04.039

[31] J. Wang, H. Pan, D. Meng, X. Wu, Y. Wang, X. Meng, Synthesis, characterization and catalytic performances of $S_2O_8^{2-}$/Al-x wt%Ce–Zn–O solid acid catalysts, *React. Kinet. Mech. Catal.* **102** (2011) 331-341. https://doi.org/10.1007/s11144-010-0276-x

[32] X. Shi, Y. Wu, P. Li, H. Yi, M. Yang, G. Wang, Catalytic conversion of xylose to furfural over the solid acid SO_4^{2-}/ZrO_2–Al_2O_3/SBA-15 catalysts, *Carbohydr. Res.* **346** (2011) 480-487. https://doi.org/10.1016/j.carres.2011.01.001

[33] X. Han, M. Bian, K. Liu, X. Yang, D. Zheng, X. Yang, Y. Zhang, Influence of Particle Size of CeO_2 Nanospheres Encapsulated in SBA-15 Mesopores on SO_2 Tolerance during NH_3-SCR Reaction, *Catalysts* **14** (2024) 151. https://doi.org/10.3390/catal14020151

[34] J. L. Ropero-Vega, A. Aldana-Pérez, R. Gómez, M. E. Nino-Gómez, Sulfated titania [TiO_2/SO_4^{2-}]: A very active solid acid catalyst for the esterification of free

fatty acids with ethanol, *Appl. Catal. A* **379** (2010) 24-29. https://doi.org/10.1016/j.apcata.2010.02.020

[35] H. H. Salam Al-Jaberi, U. Rashid, F. A. J. Al-Doghachi, G. Abdulkareem-Alsultan, Y. H. Taufiq-Yap, Synthesis of MnO-NiO-SO_4^{2-}/ZrO_2 solid acid catalyst for methyl ester production from palm fatty acid distillate, *Energy Convers. Manage.* **139** (2017) 166-174. http://dx.doi.org/10.1016/j.enconman.2017.02.056